Final Draft
of the original manuscript:

Yan, W.; Fang, L.; Noechel, U.; Gould, O.E.C.; Behl, M.; Kratz, K.; Lendlein, A.:

Investigating the Roles of Crystallizable and Glassy Switching Segments within Multiblock Copolymer Shape-Memory Materials

In: MRS Advances (2017) Cambridge University Press

DOI: 10.1557/adv.2018.590

INVESTIGATING THE ROLES OF CRYSTALLIZABLE AND GLASSY SWITCHING SEGMENTS WITHIN MULTIBLOCK COPOLYMER SHAPE-MEMORY MATERIALS

Wan Yan,[1, 2] Liang Fang,[1,3] Ulrich Noechel,[1] Oliver E. C. Gould,[1] Marc Behl,[1] Karl Kratz,[1] Andreas Lendlein[*1, 2]

[1] *Institute of Biomaterial Science and Berlin-Brandenburg Center for Regenerative Therapies, Helmholtz-Zentrum Geesthacht, Kantstr. 55, 14513 Teltow, Germany*
[2] *Institute of Chemistry, University of Potsdam, 14476 Potsdam, Germany*
[3] *Present Address: College of Material Science and Engineering, Nanjing Tech University, 210009, Nanjing, China.*

* Correspondence to:
Prof. Dr. Andreas Lendlein
Institute of Biomaterial Science, Helmholtz-Zentrum Geesthacht, Kantstr. 55, 14513 Teltow, Germany
Email: andreas.lendlein@hzg.de
Phone: +49 (0)3328 352-450
Fax: +49 (0)3328 352-452

ABSTRACT

The variation of the molecular architecture of multiblock copolymers has enabled the introduction of functional behaviour and the control of key mechanical properties. In the current study, we explore the synergistic relationship of two structural components in a shape-memory material formed of a multiblock copolymer with crystallizable poly(ε-caprolactone) and crystallizable poly[oligo(3S-iso-butylmorpholine-2,5-dione)] segments (PCL-PIBMD). The thermal and structural properties of PCL-PIBMD films were compared with PCL-PU and PIBMD-PU, investigated by means of DSC, SAXS and WAXS measurements. The shape-memory properties were quantified by cyclic, thermomechanical tensile tests, where deformation strains up to 900% were applied for programming PCL-PIBMD films at 50 °C. Toluene vapor treatment experiments demonstrated that the temporary shape was fixed mainly by glassy PIBMD domains at strains lower than 600%, with the PCL contribution to fixation increasing to 42±2% at programming strains of 900%. This study into the shape-memory mechanism of PCL-PIBMD provides insight into the structure-function relation in multiblock copolymers with both crystallizable and glassy switching segments.

Introduction

Shape memory polymers (SMPs) have been investigated intensively because of their ability to generate large changes in strain in response to external stimuli, such as temperature, magnetic field and light etc [1-8]. To exhibit a shape-memory effect a polymer network material must contain a suitable switching domain, which provides the shape fixation and driving force for the movement, and netpoints, which determine the permanent shape of the material. These netpoints can be physical or chemical cross-links, while the temporary shape can be fixed by polymer chain immobilization, commonly through vitrification or crystallization [1, 2].

Multiblock copolymers (MBCs) with two phase-separated domains can be utilized to generate a heat-induced shape-memory effect (SME). Here, an amorphous or crystalline domain with a high thermal transition temperature ($T_{trans,high}$) provides netpoints determining the permanent shape, while chain segments in domains with a lower glass or melting transition (T_g or T_m, symbolized as $T_{trans,low}$) act as molecular switches.

The permanent shape of the material can be processed at a temperature above $T_{trans,high}$. At temperatures lower than $T_{trans,high}$ but higher than $T_{trans,low}$, a secondary shape can be temporarily deformed and then fixed by cooling to a $T < T_{trans,low}$. Recovery to the permanent shape occurs when the deformed sample is reheated to $T > T_{trans,low}$ [1, 2, 9, 10].

Recent developments in synthetic chemistry have led to a diverse range of shape-memory MBCs, where the key structural functions are provided by different compositional elements either cooperatively or independently. For example in a MBC prepared from the macrodiols of poly(*L*-lactide)-diol (PLLA-diol) and poly(glycolide-*co*-*ε*-caprolactone)-diol (PGC-diol) coupled with 1,6-hexanediisocyanate, crystalline PLLA domains with a T_m of approximately 150 °C provide netpoints, while a mixed amorphous phase with a single T_g around 45 °C forms switching domains [11]. In MBCs composed of two crystallizable segments such as poly(*ω*-pentadecalactone)-poly(*ε*-caprolactone) (PPDL-PCL), crystalline phases of PPDL and PCL with T_ms of around 81 and 44 °C respectively, serve as both netpoints and switches in the shape-memory process [12, 13]. Further clarification of the roles of these different compositional elements would enable the design criteria for realization of thermoplastic shape-memory polymers with minimized creeping behavior providing an increased shelf live time of the programmed temporary state.

In this study PCL-PIBMD synthesized from equal weight amounts of oligomeric starting materials oligo(*ε*-caprolactone)-diol and oligo(3S-*iso*-butylmorpholine-2,5-dione)-diol was chosen, which has been reported to exhibit excellent thermosensitive shape-memory properties [14]. In this system, PIBMD crystals with $T_{m,PIBMD}$ of 170±2 °C act as permanent physical netpoints, while both PCL crystalline domains with $T_{m,PCL}$ = 38±2 °C and PIBMD amorphous domains with $T_{g,PIBMD}$ = 40±2 °C form molecular switches [15]. In the current study, we expand on our previous work [16] by comparing the properties of PCL-PIBMD with PCL-PU and PIBMD-PU as assessed by dynamic scanning calorimetry (DSC), in situ wide-angle X-ray scattering (WAXS) and small-angle X-ray scattering (SAXS). Shape-memory properties were evaluated via cyclic, thermomechanical tensile tests. Further, a method of toluene vapor treatment was applied in cooperation with thermomechanical tensile testing to separate the relative contributions of PCL crystalline phase and PIBMD amorphous phase to switching domains.

Experimental

Materials

PCL-PIBMD, PCL-PU and PIBMD-PU were synthesized from PCL-diol (M_n = 2700 g·mol^{-1}) and PIBMD-diol (M_n = 9300 g·mol^{-1}), which reacted with trimethyl hexamethylene diisocyanate (TMDI) using dibutyltin dilaurate as catalyst as previously described [14]. The M_n of the PCL-PIBMD product was 53000 g·mol^{-1} with a polydispersity (PD) of 2.0, while PCL-PU and PIBMD-PU exhibited a M_n of 54000 g·mol^{-1} (PD: 3.4) and 48000 g·mol^{-1} (PD: 1.7) respectively.

Film preparation

The preparation of solution casted films is exemplarily described for PCL-PIBMD. PCL-PIBMD (2.28 g) was dissolved in 50 mL chloroform overnight at ambient temperature. The solution casting was carried out in glass petri dishes (diameter = 80 mm, Duran Group, Wertheim, Germany) with subsequent evaporation of chloroform for 5 days. The resulting film thickness was 270 ± 30 µm, measured using a thickness gauge (Hans Schmidt, Waldkraiburg, Germany).

Characterization methods

Cyclic, thermomechanical tensile tests

Programming as well as cyclic, thermomechanical tensile tests consisting of three repetitive cycles were performed with test specimens type DIN EN ISO 527-2/1BB (length = 20 mm, width = 2 mm) on a tensile tester (Zwick Z1.0, Ulm, Germany) equipped with a thermo-chamber and a temperature controller (Eurotherm Regler, Limburg, Germany). Each cycle consisted of a programming procedure and a recovery module performed either under stress-free or constant-strain conditions.

For programming, test specimens were first heated to 75 °C and kept 10 min to erase the thermal history. Then the temperature was reduced to 50 °C, the specimens were deformed to a strain of ε_m = 50, 200, 600 or 900% with a strain rate of 1 mm·min^{-1}. Subsequently, the deformed specimens were kept at 50 °C for 5 min to allow relaxation. Finally, the samples were cooled to 0 °C under constant strain and the temporary shape was obtained after releasing the stress. After 10 min fixation, the programming was completed by removal of the stress, while the temporary fixed strain (ε_u) was achieved. Recovery under free-stress condition, resulting in the recovered strain (ε_p), or constant-strain conditions was induced by heating the programmed sample from 0 to 75 °C at 2 °C·min^{-1}. For quantification of the shape-memory properties, the shape fixity (R_f) and shape recovery ratio (R_r) were calculated by the following equations, where N is the present N^{th} cycle. From the obtained stress-temperature-strain curves the switching temperature T_{sw} and $T_{\sigma,max}$ as well as the maximum recovery stress (σ_{max}) were determined as described before in Ref. [17].

$$R_f = \frac{\varepsilon_u(N)}{\varepsilon_m} \quad (1)$$

$$R_r = \frac{\varepsilon_m - \varepsilon_p(N)}{\varepsilon_m - \varepsilon_p(N-1)} \quad (2)$$

In this work, only the first cycle of each measurement was analysed as here the samples exhibited the identical thermomechanical history as the original samples. Thus the system errors from the thermal control and stress detecting of the tensile test machine were considered. The estimated error for R_f and R_r was ±2%, for the determined characteristic switching temperatures ±2 °C and for the stress ±5%.

Differential scanning calorimetry (DSC)

DSC experiments were conducted on a Netzsch DSC 204 Phoenix (Selb, Germany) at a heating rate of 10 °C·min^{-1} in sealed aluminum pans. The polymer samples were cooled down from room temperature to 0 ºC before they were heated to 200 ºC, while the T_m and related melting enthalpies (ΔH) were determined from DSC curves. A non-deformed PCL-PIBMD sample was measured after being preconditioned by annealing at 75 °C for 10 min, then cooling down to 50 °C and keeping for 10 min at T_{deform}, and afterwards cooling to 0 °C with a cooling rate of 5 °C·min^{-1} by using DSC to simulate the main thermal treatment applied during programming. The deformed samples were prepared as described above.

Dynamic mechanical thermal analysis (DMTA)

DMTA measurement was carried on an Eplexor 25 N (Gabo, Ahlden, Germany) equipped with a 25 N load cell using the standard type test specimen (DIN EN ISO 527-2/1BB). The applied oscillation frequency was 1 Hz. The measurement was performed in the temperature sweep mode from -100 °C to 200 °C with a constant heating rate of 2 °C·min^{-1}. The T_g was determined at the peak maximum of tan δ *vs* temperature curve.

Wide- and Small angle X-ray scattering (WAXS, SAXS)

WAXS measurements were performed on a Bruker D8 Discover X-ray diffraction system with a two-dimensional detector from Bruker AXS (Karlsruhe, Germany). A custom build tensile device was used for uniaxial deformation of PCL-PIBMD samples. Heating was provided by a heating gun (heating rate ~10 °C·min^{-1}, non-linear), whereby cooling was enabled by a stream of gaseous nitrogen, which was passed through a serpentine shaped metal tube submerged in liquid nitrogen (Cooling rate ~10 °C·min^{-1}, non-linear). The temperature was monitored by a thermocouple touching the sample. For *in situ* WAXS measurements, the samples were initially programmed under the designed conditions. Then the programmed samples were fixed in the sample holder and WAXS patterns were recorded at 0 and 50 °C with an exposure time of 120 s per scattering pattern. The relationship of the integrated areas of crystalline and amorphous region determines the overall degree of crystallinity (*DOC*) according to Equation (3). The lateral crystal size (l_c) was calculated according the Sherrer equation (4) [18].

$$DOC = \frac{A_{cryst}}{A_{cryst} + A_{amorp\ h}} \times 100 \quad (3)$$

$$l_c = \frac{k \times \lambda}{B \times \cos\theta} \quad (4)$$

Where λ is the wavelength of the applied X-rays (0.15418 nm), parameter k = 0.9, B is full width at half maximum (in radians) and θ is the half scattering angle. We estimated the error for l_c to ±0.2 nm.

SAXS experiments were performed on a Bruker Nanostar diffractometer (Bruker AXS, Karlsruhe, Germany), using a 400 µm beam with a wavelength of 0.15418 nm (CuKα) and a Vantec-2000 detector (2048*2048 pixel, 68 µm pixel size) to record scattered intensities at a distance of 1050 mm from the samples. The samples were initially programmed under the designed conditions. Then the programmed samples were fixed in the sample holder and exposed 1 h to obtain a two dimensional scattering pattern at 0 and 50 °C. The obtained anisotropic scattering patterns were integrated over a 10° wide azimuthal range along the axis of symmetry (fiber axis, s_3). The long period L was extracted from the position of the peak maxima of the Kratky-plot after Lorenz correction Is^2 vs. s, where s is the scattering vector as $L = s^{-1}$ [19]. The error for L was estimated as ±0.2 nm.

Toluene vapor treatment

A glass cylinder (height 20 cm, diameter 10 cm) was designed and produced to be installed in the thermomechanical tensile test machine, in which the samples were measured. After the programming procedure, 3 ml toluene was injected into the cylinder to form the environment with saturated toluene vapor. The deformed specimens were placed in the toluene vapor for 1 h, followed by heating to 75 °C to allow complete recovery. The changes in length of deformed specimens were recorded by the thermomechanical tensile testing machine. The recovery ratio in toluene vapor, $R_{r,toluene}$, and the final recovery ratio after heating, $R_{r,heating}$, were calculated according to equation (5) and (6).

$$R_{r,toluene} = \frac{\varepsilon_m - \varepsilon_{toluene}}{\varepsilon_m} \quad (5)$$

$$R_{r,heating} = \frac{\varepsilon_m - \varepsilon_{heating}}{\varepsilon_m} \quad (6)$$

where $\varepsilon_{toluene}$ and $\varepsilon_{heating}$ is the strain of sample after toluene vapor treatment and heating to 75 °C.

Results and discussion

The thermal properties and morphology of PCL-PIBMD films were compared with polyurethanes prepared by reaction of PCL-diol (PCL-PU) or PIBMD-diol (PIBMD-PU) with TMDI investigated by means of DSC, SAXS and WAXS measurements. The obtained results are listed in **Table 1**.

PCL-PU showed a melting peak at 49±1 °C with a $T_{g,PCL}$ located at -64±1 °C, while the PIBMD-PU had a cold crystallization peak at 126±1 °C and a melting peak at 167±1 °C with a glass transition at 48±1 °C. Compared to PCL-PU and PIBMD-PU, two distinct T_ms of PCL-PIBMD were observed at 39±1 and 168±1 °C in the second scan, which are attributed to PCL and PIBMD crystalline phases, respectively. Here, the PIBMD melting peak is relatively unchanged from its PIBMD-PU, however the PCL melting peak is significantly lower in the PCL-PIBMD. Further, the influence of PIBMD on the crystallization behavior of PCL domains is also visible in the $\Delta H_{m,PCL}$ value, which was measured as 2±2 J·g^{-1} in PCL-PIBMD, a significantly smaller value than that obtained for PCL-PU (51±2 J·g^{-1}). This effect is likely to be the result of the restriction of PIBMD crystals on the crystallization of PCL domains, as reported in previous work [20]. Since $T_{g,PIBMD}$ of PIBMD-PU overlapped with the melting peak of crystalline PCL domains, DMTA was used for the further determination of $T_{g,PIBMD}$ in PCL-PIBMD.

Table 1. Thermal properties of PCL-PU, PIBMD-PU and PCL-PIBMD films obtained from DSC and DMTA measurements.

Samples	$T_{m,PCL}$	$\Delta H_{m,PCL}$	$T_{c,PCL}$	$T_{g,PCL}$	$T_{m,PIBMD}$	$\Delta H_{m,PIBMD}$	$T_{cc,PIBMD}$	$T_{g,PIBMD}$
	ºC	J·g^{-1}	ºC	ºC	ºC	J·g^{-1}	ºC	ºC
PCL-PU	49±1	51±2	24±1	-64±1	-	-	-	-
PIBMD-PU	-	-	-	-	167±1	16±2	126±1	48±1

PCL-PIBMD first scan	-	16±2	-	-	167±1	22±2	-	32±3*
PCL-PIBMD second scan	39±1	2±2	-	-59±1	168±1	17±2	108±1	-

Note: $T_{m,PCL}$, $\Delta H_{m,PCL}$, $T_{c,PCL}$, $T_{g,PCL}$, $T_{m,PIBMD}$, $\Delta H_{m,PIBMD}$ and $T_{cc,PIBMD}$ were obtained from DSC measurement; The estimated error for T is ±1 °C and for ΔH is ±2 J·g^{-1}.
*$T_{g,PIBMD}$ was obtained from DMTA measurement with a estimated error of 3 °C.

WAXS and SAXS were performed to study the crystal structures of PCL-PIBMD films. Calculations based on the SAXS profiles taken at 25 and 75 °C illustrated the lamellar structure in PCL-PIBMD films, with a long period of 13.0±0.2 nm at 25 °C, which increased to 14.0±0.2 nm after heating to 75°, as shown in **Table 2**. This result agrees with the confinement of PCL crystals within the PIBMD crystal lamellae as observed in previously published AFM data [16]. By comparing the WAXS intensity profiles of PCL-PU and PIBMD-PU, PCL-PIBMD films in **Figure 1** show several peaks that can be attributed to the crystal structures of PIBMD at 2θ = 8.8, 17.5, 19.1, 21.6, 23.9 and 26.0º, which overlapped with typical PCL crystal patterns in (110) and (200) at 21.3 and 23.8º, respectively. Here, as listed in **Table 2**, the size of PIBMD crystals was calculated from the diffraction peak at 8.8º, which can be considered as the characteristic peak of PIBMD crystals, while the PCL crystal size at 0 °C was roughly calculated from its characteristic pattern (110) at 21.3°, neglecting the influence from PIBMD pattern. The PCL-PIBMD films had a degree of crystallinity (*DOC*) around 28±2% at 20 °C, which decreased to 25±2% with the melting of the PCL crystals during the heating to 75 °C.

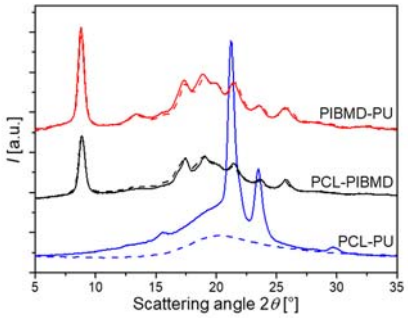

Figure 1. 2D WAXS profiles of PCL-PU (blue), PIBMD-PU (red) and PCL-PIBMD (black) films sample at 0 °C (solid line) and 75 °C (dash line).

Table 2. Crystal structure of PCL-PIBMD films obtained from WAXS and SAXS measurements.

Temperature	L	$l_{c,PIBMD}$	$l_{c,PCL}$	DOC
°C	nm	nm	nm	%
20	13.0±0.2	16.4±0.2	8.0±0.2	28±2
75	14.0±0.2	16.0±0.2	-	25±2

Note: L was calculated from SAXS measurement with an estimated error of 0.2 nm; $l_{c,PIBMD}$ and $l_{c,PCL}$ were obtained from WAXS measurement with an estimated error of 0.2 nm.

Strains of 50, 200, 600, and 900% were applied to evaluate the shape-memory properties of PCL-PIBMD films. The stress-temperature-strain curves of the first cycle are shown in **Figure 2**. T_{deform} was chosen as 50 ºC, higher than both $T_{m,PCL}$ and $T_{g,PIBMD}$, while the strain rate was 1 mm·min^{-1}. The deformed shapes were then fixed by cooling to 0 °C. Afterwards, the stress-free (**Figure 2a)** or constant-strain (**Figure 2b)** recovery was activated by increasing the temperature to 75 ºC.

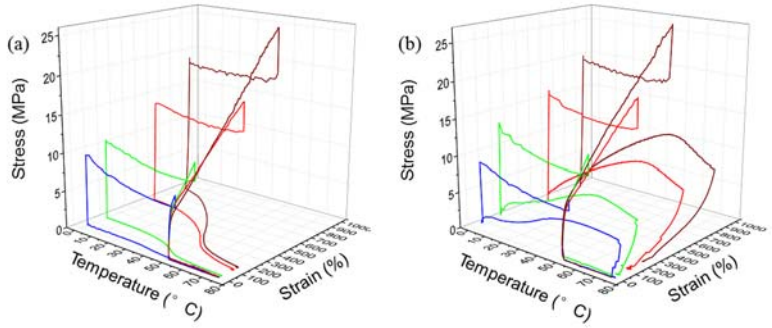

Figure 2. The first cycle curves of cyclic tests of PCL-PIBMD films programmed to strain of 50 (blue), 200 (green), 600 (red) and 900% (brown) at 50 °C and recovered under (a) stress-free and (b) constant-strain conditions.

In PCL-PIBMD both the amorphous PIBMD phase and PCL domains can act as switching domains. By dissolving the PCL crystals at 0 °C, toluene can be used to decouple the relative contributions of the two structural units to the shape memory mechanism. With the removal of the PCL crystals, the recovery of the original shape is solely prevented by the glassy PIBMD phase. After the PCL-PIBMD samples were deformed to strains of 50, 200, 600 and 900% at 50 °C and fixed by cooling at 0 °C, toluene was injected into a glass cylinder containing the deformed samples. After a 1 h recovery in toluene vapor, the samples were heated to 75 °C to allow the complete melting of both PCL and PIBMD, and the material's full recovery. An example measurement at 900% strain is shown in **Figure 3a,** and the combined results are summarized in **Table 3.** At a programming strain of 200%, the PCL crystalline phase only contributed around 6±2% to the whole recovery ratio, while this ratio increased to 42±2% at a programming strain of 900%. Additional DSC tests, as shown in **Figure 3b,** were performed to examine the deformed PCL-PIBMD samples after toluene vapor treatment. No PCL melting peak can be found in the heating scans, suggesting that the PCL crystals which fixed the temporary shape were eliminated in toluene, while peaks from the PIBMD crystals were not changed by the toluene vapor.

These results indicate that the vitrification of the amorphous PIBMD phase is the main contributor to the fixation of temporary shape. However, at higher strains where PCL amorphous chains are highly stretched, the contribution from PCL crystals to the switching domains increases dramatically. We postulate that deformation to higher strain values causes the fragmentation of the PIBMD domains and facilitates the formation of chain-extended PCL crystals, which provide a greater contribution to the switching domains and lead to the observed increase in T_{sw}.

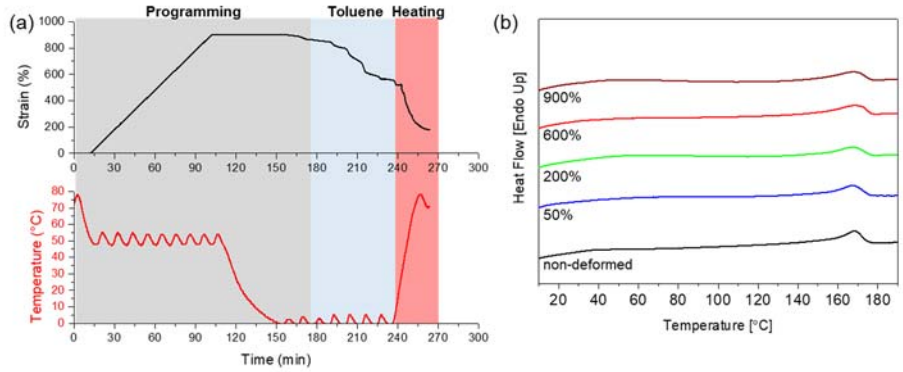

Figure 3. (a) Recovery process combined with toluene vapor treatment in thermomechanical tensile test when PCL-PIBMD was programmed to 900% at 50 °C. (b) DSC 1st heating curve of PCL-PIBMD films deformed to strain of 0% (black), 50% (blue), 200% (green), 600% (red) and 900 % (brown) at 50 °C and then recovered in toluene vapor.

Table 3. Shape-memory properties for PCL-PIBMD films programmed to 50, 200, 600 and 900% strain at 50 °C.

Strain	R_f	R_r	T_{sw}	$\sigma(\varepsilon_m)$	σ_{max}	$\sigma_{max}/\sigma(\varepsilon_m)$	$T_{\sigma,max}$	$R_{r,\,toluene}$	$R_{r,\,heating}$
[%]	[%]	[%]	[ºC]	[MPa]	[MPa]	[%]	[ºC]	[%]	[%]
50%*	93±2	92±2	36±2	7.5±0.4	4.9±0.2	65±4	56±2	18±2	80±2
200%*	96±1	89±1	42±1	12.4±0.6	7.4±0.4	60±3	57±2	6±2	63±2
600%	97±2	82±2	43±2	17.7±0.9	9.4±0.5	53±6	58±2	16±2	73±2
900%	94±1	82±2	41±2	26.4±1.3	11.4±0.6	43±4	55±2	42±2	80±2

Note: The R_f, R_r, T_{sw}, were determined as the average of three cycles measurement under stress-free recovery; $\sigma(\varepsilon_m)$, σ_{max}, $\sigma_{max}/\sigma(\varepsilon_m)$ and $T_{\sigma,max}$ were determined from the 1st cycle measurement under constant-strain recovery. The estimated errors for R_f and R_r is ±2%, for T is ±2 °C and for σ is ±5%. $R_{r,\,toluene}$ and $R_{r,\,heating}$ was determined by the continuous measurement in toluene vapor and by heating after deformation with an estimated error of ±2%. *Shape-memory values, excluding $R_{r,\,toluene}$ and $R_{r,\,heating}$, for these two deformation strains are shown from ref [16] and [15] for comparison.

Conclusions

In this study we investigate the shape-memory mechanism of PCL-PIBMD, a shape-memory polymer with both crystallizable and glassy switching segments. By providing several new insights into the contributions of the different structural elements, specifically by DSC, WAXS and SAXS measurement and under toluene vapor treatment, we are able to build a more complete picture of the often complex behavior of shape-memory MBCs. This greater understanding should aid the development of a compositionally diverse range of thermoplastic shape-memory materials with minimized creeping behavior providing an increased shelf live time of the programmed temporary state.

Acknowledgements

This work was supported by the Helmholtz-Association through programme-oriented funding. The authors thank Mr. Olaf Lettau for technical support. W. Yan acknowledges the German Federal Ministry for Education and Research (BMBF, Grant No. 031A095) for financial support.

References

1. K. K. Julich-Gruner, C. Löwenberg, A. T. Neffe, M. Behl and A. Lendlein, *Macromolecular Chemistry and Physics* **214** (5), 527-536 (2012).
2. M. Behl, U. Ridder, Y. Feng, S. Kelch and A. Lendlein, *Soft Matter* **5** (3), 676-684 (2009).
3. T. Xie, *Polymer* **52** (22), 4985-5000 (2011).
4. J. Hu, Y. Zhu, H. Huang and J. Lu, *Progress in Polymer Science* **37** (12), 1720-1763 (2012).
5. X. J. Han, Z. Q. Dong, M. M. Fan, Y. Liu, Y. F. Wang, Q. J. Yuan, B. J. Li and S. Zhang, *Macromolecular rapid communications* **33** (12), 1055-1060 (2012).
6. A. Lendlein, H. Jiang, O. Jünger and R. Langer, *Nature* **434** (7035), 879-882 (2005).
7. M. Y. Razzaq, M. Anhalt, L. Frormann and B. Weidenfeller, *Materials Science and Engineering: A* **444** (1), 227-235 (2007).
8. M. Y. Razzaq and L. Frormann, *Polymer Composites* **28** (3), 287-293 (2007).
9. A. Lendlein and S. Kelch, *Angewandte Chemie International Edition* **41** (12), 2034-2057 (2002).
10. P. T. Mather, X. Luo and I. A. Rousseau, *Annual Review of Materials Research* **39**, 445-471 (2009).
11. C. Min, W. Cui, J. Bei and S. Wang, *Polymers for Advanced Technologies* **16** (8), 608-615 (2005).
12. K. Kratz, U. Voigt and A. Lendlein, *Advanced Functional Materials* **22** (14), 3057-3065 (2012).
13. H. Matsumoto, T. Ishiguro, Y. Konosu, M. Minagawa, A. Tanioka, K. Richau, K. Kratz and A. Lendlein, *European Polymer Journal* **48** (11), 1866-1874 (2012).
14. Y. Feng, M. Behl, S. Kelch and A. Lendlein, *Macromolecular Bioscience* **9** (1), 45-54 (2009).
15. W. Yan, L. Fang, U. Noechel, K. Kratz and A. Lendlein, *Express Polymer Letters* **9** (7), 624-635 (2015).
16. W. Yan, L. Fang, U. Noechel, K. Kratz and A. Lendlein, *Journal of Polymer Science Part B: Polymer Physics* **54** (19), 1935-1943 (2016).
17. T. Sauter, M. Heuchel, K. Kratz and A. Lendlein, *Polymer Reviews* **53** (1), 6-40 (2013).
18. P. Scherrer, *Bestimmung der inneren Struktur und der Größe von Kolloidteilchen mittels Röntgenstrahlen. In: Kolloidchemie Ein Lehrbuch, Chemische Technologie in Einzeldarstellungen*. (Springer, Berlin, 1912).
19. N. Stribeck, *X-ray scattering of soft matter*. (Springer Science & Business Media, Berlin, 2007).
20. W. Yan, T. Rudolph, U. Noechel, O. Gould, M. Behl, K. Kratz and A. Lendlein, *Macromolecules* **51** (12), 4624-4632 (2018).